Fall Detection in Ambient-Assisted Living Environments Using FMCW Radars and Deep Learning

Fall Detection in Ambient-Assisted Living Environments using FMCW Radars and Deep Learning

Ali Samimi Fard[1] Mohammadreza Mashhadigholamali[1] Samaneh Zolfaghari[2] Hajar Abedi[3] Mainak Chakraborty[2] Sachin Karmani[3] Luigi Borzì[1] Masoud Daneshtalab[2] George Shaker[3]

[1] *Department of Control and Computer Engineering, Politecnico di Torino, Turin, Italy.*
Email: {ali.samimifard, mohammadreza.mashhadigholami}@studenti.polito.it, luigi.borzi@polito.it

[2] *School of Innovation, Design and Engineering, Mälardalen University, Västerås, Sweden.*
Email: {samaneh.zolfaghari, mainak.chakraborty,masoud.daneshtalab}@mdu.se

[3] *Department of Electrical and Computer Engineering, University of Waterloo, Ontario, Canada.*
Email: {habedifi, skarmani, gshaker}@uwaterloo.ca

***Abstract*—The global rise in the elderly population has increased the demand for effective fall detection in Ambient Assisted Living (AAL) environments. This paper introduces a novel and reliable fall detection system utilizing frequency-modulated continuous wave (FMCW) radar, designed to address privacy concerns, operate reliably in low-light conditions, and provide ease of installation. Data from two wall-mounted radars capture a variety of activities, including simulated falls, across five configurations to enhance model generalizability. Radar data processing employs the Fast Fourier Transform (FFT) and the Capon algorithm to generate Range-Azimuth and Range-Elevation maps, which serve as input features for a proposed 3D Convolutional Neural Network (3D CNN) model. This model achieves an accuracy of 94.33% and F1-score of 93.5%, combining high performance with adaptability across diverse environments and user needs. This work provides a robust solution for fall detection with significant potential for deployment in real-world elderly care settings.**

***Index Terms*—fall detection, mmWave, FMCW radar, deep learning, elderly care, ambient assisted living**

I. Introduction

The rapid growth of the elderly population has become a significant global challenge, leading to various health and safety concerns. Falls are a major cause of injury among elderly individuals, especially those living in independent or long-term care settings [1]. Research indicates that most elderly individuals who experience a fall are unable to rise unassisted, and those who remain on the ground for extended periods are at significantly higher risk of death within six months, even if no serious injuries occur. Thus, prompt detection of falls is essential for minimizing long-term health consequences, enabling timely medical intervention, and improving the overall quality of life in Ambient Assisted Living (AAL) environments [2].

The development of fall detection systems has been a significant research focus in recent decades [1]. Many of these systems rely on wearable devices; however, such sensors often pose issues related to user compliance, comfort, and convenience. These devices can be cumbersome, leading to inconsistent use or outright rejection by elderly individuals [3].

Non-wearable approaches have recently attracted significant attention as they offer a less intrusive alternative to wearable devices by integrating sensors into the living environment. These systems provide the advantage of not restricting users' movements, enhancing comfort and ease of use. However, non-wearable approaches also present limitations, such as privacy concerns, limited operational range, and reduced performance in low-light conditions [4].

Millimeter wave (mmWave) radars, particularly frequency-modulated continuous wave (FMCW) radars, have emerged as a promising alternative for fall detection in such contexts. These radar systems ensure privacy preservation, are easy to install, and operate reliably in low-light environments [4]. Additionally, mmWave radars can detect human movement through wall-mounted setups, providing robust continuous monitoring in AAL environments without compromising user comfort or safety. FMCW radars transmit signals whose frequency increases linearly over a fixed time interval, allowing simultaneous measurement of the target's range, velocity, and angle [5]. As such, FMCW radars are highly effective for in-home activity monitoring. Their performance has been evaluated in applications such as human activity recognition [4], [6], [7], gait analysis [8], [9], and fall detection [10]. Moreover, multiple FMCW radars can be deployed in close proximity, making them ideal for large-scale monitoring in settings like long-term care facilities [11]. This paper introduces a novel fall detection system that leverages FMCW radars and deep learning to address the growing demand for scalable fall detection solutions for elderly care. The proposed system employs two wall-mounted FMCW radars to capture human activities. Then, radar data is processed using the Fast Fourier Transform (FFT) and the Capon algorithm to generate Range-Azimuth (RA) and Range-Elevation (RE) maps, which serve as input features for a 3D Convolutional Neural Network (3D CNN). This approach provides advantages over Doppler-based

methods, including improved accuracy, fewer false positives, and greater generalizability across environments. The proposed system achieves high accuracy and computational efficiency, making it suitable for deployment in AAL environments.

II. Proposed System Prototype

Fig. 1 illustrates an overview of the proposed system prototype for fall detection. In the following sections, we will explore each module in detail.

A. Radar Setup and Data Collection

In this study, we employed the mmWave FMCW radar system BGT60TR13C, developed by Infineon Technologies AG. This radar operates at frequencies between 58 and 63.5 GHz, transmitting signals via one transmitter and receiving reflections through three receivers. Table I provides a detailed overview of the radar configuration used in this paper. Due to the L-shaped architecture of the radar antenna array, it can measure both horizontal (azimuth) and vertical (elevation) angles, in addition to capturing velocity and range information from the target [12].

TABLE I: Radar Configuration and Specification

Parameters	Value
Radar Model	BGT60TR13C
Start Frequency	61 GHz
End Frequency	61.5 GHz
Transmit Output Power	5 dBm
ADC Sampling Rate	2 Msps
Frame Rate	10
Chirps Per Frame	128
Number of Tx Antennas	1
Number of Rx Antennas	3
Range resolution	30 cm
Max Unambiguous Range	4.8 m

To collect the data, two radar devices were installed at a height of 210 cm above the ground—one positioned above a window and the other above a television. Both devices were installed at a 30-degree tilt to maximize the room coverage. Eleven healthy subjects participated in the study, each performing three specific activities in the room. All participants completed every activity in each of the five predefined positions in the living room, as illustrated in Fig. 2.

This study investigates the binary classification of fall and non-fall scenarios. For the non-fall scenario, two specific activities are considered: sitting on a sofa and lying on a sofa, while the fall scenario is represented by lying on the floor. These activities were chosen due to the relative ease of distinguishing between static and dynamic activities, as opposed to the more complex task of differentiating between similar static activities. Although Doppler signatures are a promising feature for fall detection, the Doppler signature of certain fall types can resemble other movements, such as sitting, making it difficult to differentiate between them. Furthermore, the Doppler signature of the same activity varies when observed from different angles. Therefore, relying solely on Doppler information can lead to a high rate of false alarms, reducing the effectiveness of the model for fall detection [13], [14].

Due to ethical and practical constraints, actual fall data are not collected, as inducing falls in human participants would pose significant safety risks [15]. Instead, lying on the floor is used as a surrogate for a fall scenario. This substitution is based on the observation that lying on the floor is rare, particularly in residential care units, where it is often linked to adverse events, including falls. Therefore, detecting an individual lying on the floor is a practical and reliable indicator of a fall [16].

Existing research supports this approach, demonstrating that the inability to rise after a fall is a crucial marker of fall-related incidents, particularly among older adults. For instance, one study indicated that approximately 80% of individuals aged 90 or older are unable to get up after a fall, with many remaining on the floor for extended periods due to a lack of assistance or cognitive impairment [17]. Additionally, most existing datasets for fall detection are collected from young, healthy participants simulating falls. For safety, these simulations are typically conducted on mattresses. However, in real-life falls, people often instinctively try to break their fall with their hands—a reaction that is not accurately reproduced in controlled trial settings. As a result, these datasets may not fully represent real-world fall incidents, thereby limiting the generalizability of the developed models [2]. By utilizing lying on the floor as an approximation of falls, this methodology ensures participant safety while maintaining the relevance of the dataset for practical applications, such as AAL environments where timely intervention is crucial.

The designated laboratory approved the data collection procedures at the The Schlegel-UW Research Institute for Aging (RIA), and all activities complied with the relevant safety protocols and ethical guidelines. Data collection sessions are segmented by activity type to ensure controlled and consistent conditions for each activity.

B. Preprocessing and Feature Extraction

In FMCW radars, the transmitter (TX) antenna emits a series of chirp signals, and the receiver (RX) antennas capture signals reflected from surrounding objects. The collected data is structured into a matrix with dimensions $C \times N \times M$, where C represents the number of channels, N denotes the number of chirps per frame, and M corresponds to the samples per chirp. Each row of this matrix, termed *fast time*, contains data from individual chirp, while each column, termed *slow time*, represents data from the same sample across chirps. To ensure a comprehensive analysis of each activity, preprocessing was applied separately to data from both radars. Feature maps were extracted independently from each radar without data fusion. The model was subsequently trained using all extracted feature maps.

The preprocessing stage involves several steps to enhance signal quality. First, DC bias is removed to eliminate low-frequency artifacts, and the Blackman-Harris window function is applied to reduce spectral leakage [18]. As chirp signals

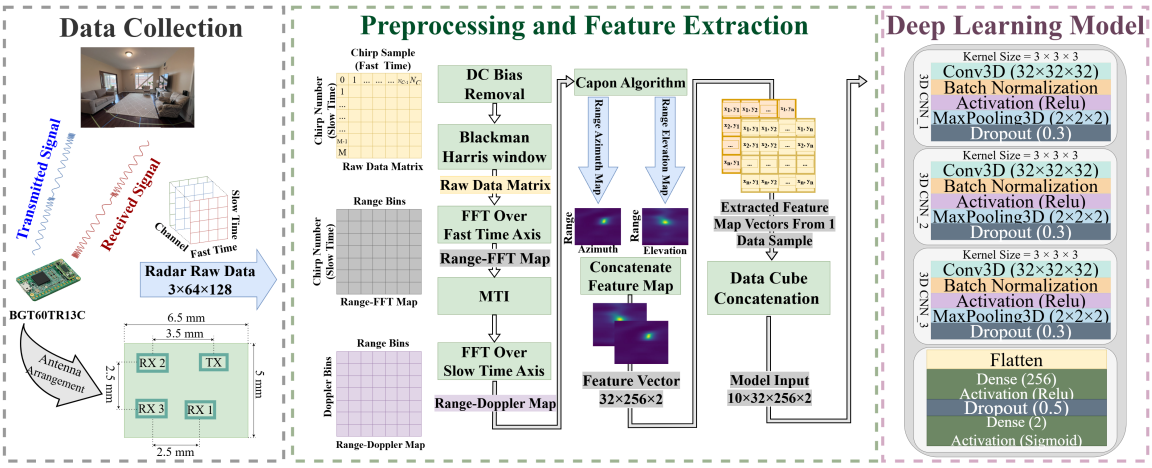

Fig. 1: Overview of the proposed system.

Fig. 2: Room layout indicating radars positions and activity locations.

increase in frequency over time, the delay between signal transmission and reception introduces both frequency and phase shifts in the received signal. Because electromagnetic waves travel at nearly the speed of light, the distance to the target can be derived from the frequency shift in the received signal.

When multiple objects are located at different distances, each reflected signal exhibits a distinct frequency shift. To separate these signals, the FFT is applied to isolate peaks within the frequency spectrum; this process is known as Range-FFT [19], [20]. Object range detection is accomplished by applying the FFT along the fast-time dimension, where the peak magnitudes in the resulting spectrum correspond to the distances of the targets. The radar emits two chirps separated by a time interval to measure target velocity. Each chirp reflection undergoes Range-FFT to determine the target distance. Although the Range-FFT peaks appear at the same locations for each chirp, the phases of these peaks differ due to target motion. The phase difference between these peaks indicates the target's velocity [19]. However, measuring higher velocities necessitates shorter intervals between chirps [21], demonstrating a trade-off between range and temporal resolution in velocity measurements.

A Moving Target Indicator (MTI) filter is applied to suppress reflections from stationary objects. This filter combines each range bin's peak across slow time ($r_{i,\max}$) with the previous output (t_{i-1}) using a weighting coefficient α:

$$t_i = \alpha \cdot r_{i,\max} + (1-\alpha) \cdot t_{i-1} \tag{1}$$

where the initial condition is $t_0 = 0$. The filtered FFT value $r_{i,\text{filt}}$ is calculated as the absolute difference between the current peak and the previous filter output [22]:

$$r_{i,\text{filt}} = |r_{i,\max} - t_{i-1}| \tag{2}$$

this MTI filtering attenuates static targets while retaining signals from moving objects.

After MTI filtering, a sequence of chirps forms a chirp frame, enabling a second FFT along the slow-time dimension to extract Doppler information. This information is combined across channels to produce a Range-Doppler map. To locate objects in three-dimensional (3D) space, both range and angle must be determined. Multipath propagation can distort the range profile by introducing multiple reflection paths [8]. The Capon algorithm is applied to the Range-Doppler data, enabling the generation of precise Range-Azimuth (RA) and Range-Elevation (RE) maps [23].

The Capon algorithm estimates the Angle of Arrival (AoA) by solving an optimization problem that minimizes the output power P_{out} while ensuring a distortionless response in the desired target direction:

$$\min_{\mathbf{w}} \left(P_{\text{out}} = \frac{1}{2} \mathbf{w}^H \mathbf{R}_{xx} \mathbf{w} \right) \quad \text{s.t.} \quad \mathbf{w}^H \mathbf{a}(\theta) = 1 \tag{3}$$

where $\mathbf{R}_{xx}$ is the correlation matrix, $\mathbf{w}$ is the weight vector, and $\mathbf{a}(\theta)$ represents the steering vector at angle θ. The angular power spectrum is then computed as:

$$P_{CP}(\theta) = \frac{1}{\mathbf{a}^H(\theta) \mathbf{R}_{xx}^{-1} \mathbf{a}(\theta)} \tag{4}$$

Here, $P_{CP}(\theta)$ represents the power output at angle θ, with peaks in the spectrum corresponding to target directions, and the peak magnitudes indicating signal strength. The Capon algorithm acts as a spatial filter, enhancing signals from

desired directions while suppressing interference from others. By combining angular data from the Capon beamformer with range data from the Range-FFT, we construct RA and RE feature maps. Fig. 3 illustrates an example of a participant performing each specified scenarios with corresponding feature maps.

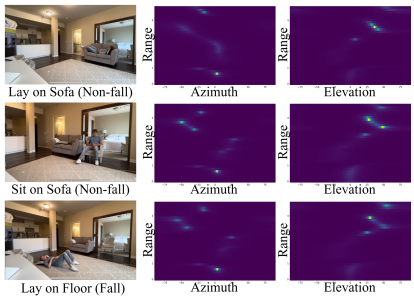

Fig. 3: Examples of a participant performing the activities with corresponding feature maps.

Following the calculation of RA and RE feature vectors, we concatenate these vectors to form a 3D data structure, referred to as a *data cube*. Subsequently, each set of ten consecutive data cubes is merged. This feature vector integrates range, azimuth, and elevation information, along with temporal data, effectively capturing spatial and temporal characteristics in a compact representation.

C. Proposed Deep Learning Model Architecture

Given the data's 3D structure, we used a 3D CNN to process spatial and temporal features within the data cubes. The 3D CNN is particularly suited for this task, as it captures both spatial and temporal dimensions across three axes, whereas traditional 2D CNNs are limited to spatial information only. This capability is crucial for our application, where accurately classifying activities like sitting and lying requires capturing temporal dynamics and spatial patterns within RA and RE maps. Moreover, due to the inherent similarities between radar-based RA and RE maps, it is challenging to distinguish subtle patterns and extract meaningful features solely through conventional methods. Deep learning models, such as CNNs, help reveal hidden information within these feature maps, allowing the model to generalize more effectively and perform robustly in real-world applications. This robustness is essential, as it allows the model to adapt to small environmental changes that may otherwise alter the feature maps, ensuring consistent performance across different settings. Our approach aligns with prior studies that have demonstrated the effectiveness of 3D CNNs in applications like continuous hand gesture recognition [24], fall detection [25] and human action recognition [26].

For training, a learning rate of *0.0001*, a batch size of *8*, and a maximum of *200* epochs were set as hyperparameters. An early stopping criterion with patience set to *20* epochs was employed to prevent overfitting, allowing training to halt if performance ceased to improve. The *Stochastic Gradient Descent (SGD)* optimizer with a momentum of *0.9* and weight decay of *1e-4* was selected to optimize the learning process, along with the *Binary Cross-Entropy* loss function, chosen for its suitability in binary classification tasks. These hyperparameters were determined through a grid search method, allowing for systematic tuning to identify the optimal configuration for the model's performance.

1) Data Normalization: Prior to training, data normalization was applied to ensure consistency across the dataset and to facilitate model convergence. The mean and standard deviation for each channel were computed from the training-validation set and then used to normalize both the training-validation and test sets.

2) Data Augmentation: Several data augmentation techniques were applied during training to enhance the model's robustness and generalization. These augmentations include Gaussian noise with a mean of *0* and a standard deviation of *0.1*, added with a probability of *0.5*. Additionally, a time-warping (scaling) augmentation was applied, in which data samples were scaled by a factor randomly chosen between *0.9* and *1.1*, with a probability of *0.5*.

III. Experimental Results and Analysis

A. Setup

The experiments were conducted on a system equipped with an AMD Ryzen *7 6800H* processor, *32* GB of RAM, and an NVIDIA GeForce RTX *3060* GPU, running Windows *11*. Python version *3.8.19* and TensorFlow version *2.10* were used to implement and execute the deep learning model. The model was trained and validated on data collected from 10 subjects, with 80% of the data used for training and the remaining 20% for validation. An evaluation is conducted on data from an additional, unseen subject to assess the model's generalization capability. The total number of samples considered for fall and non-fall scenario is presented in Table II.

TABLE II: Total sample count for each scenario

Scenario	Train	Validation	Test
Fall	96,870	24,220	12,500
Non-fall	196,920	49,240	25,000
Total	**293,790**	**73,460**	**37,500**

B. Experimental Results

The experimental methodology was designed to comprehensively evaluate both the performance metrics and computational efficiency of our proposed fall detection system across multiple configurations and input modalities. Specifically, our investigation focused on two primary aspects: (1) the impact of varying the number of 3D CNN blocks and (2) a comparative analysis of three distinct input configurations—RE, RA, and the combined as RE+RA approach.

Table III provides a comprehensive comparison of the model's performance across different configurations. The RE+RA input consistently exhibited superior performance, achieving the highest accuracy across various 3D CNN block arrangements. The model reached a peak accuracy of 94.33%

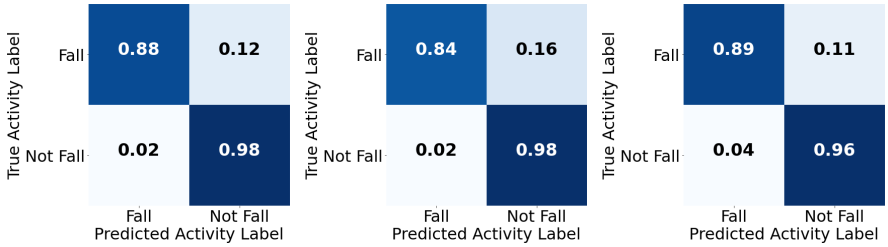

(a) One 3D CNN block. (b) Two 3D CNN blocks. (c) Three 3D CNN blocks.

Fig. 4: Normalized confusion matrices for different proposed model configurations and the RE+RA feature input.

TABLE III: Comparison of proposed 3D CNN model performance for various configurations.

# of Proposed 3D CNN Blocks	Metrics (%)	Features		
		RE	RA	RE+RA
1	**Accuracy**	89.04	81.38	94.33
	Precision	88.98	81.03	94.36
	Recall	89.04	81.38	94.33
	F1-score	87.59	78.42	93.5
2	**Accuracy**	87.9	82.74	93.45
	Precision	87.78	82.45	93.61
	Recall	87.9	82.74	93.45
	F1-score	86.19	79.69	92.38
3	**Accuracy**	87.39	83.01	93.61
	Precision	87.26	82.89	93.58
	Recall	87.39	83.01	93.61
	F1-score	85.43	79.59	92.75

with one 3D CNN block. Although adding additional 3D CNN blocks resulted in slight variations in performance, the RE+RA input maintained the highest accuracy levels, significantly outperforming models with either RE or RA inputs alone. Fig. 4a, 4b, and 4c illustrate the normalized confusion matrices for the RE+RA input configuration with one, two, and three 3D CNN blocks, respectively.

The training progression, illustrated by loss plots for different proposed 3D CNN block configurations in Fig. 5, showed that increasing the number of 3D CNN blocks enhanced convergence characteristics, indicating greater model stability during training, particularly in configurations with multiple blocks.

C. Computational Efficiency

A comprehensive analysis of computational requirements is presented in Table IV. The relationship between 3D CNN block quantity and computational demands revealed notable trends: (1) increasing the number of 3D CNN blocks led to higher floating-point operations per second (FLOPs) and increased memory consumption, and (2) the parameter count decreased with additional 3D CNN blocks due to architectural adjustments, such as the introduction of pooling layers. Across all configurations, the RE+RA input required the most memory allocation and processing time. In this paper, FLOPs is measured in GigaFLOPS (GFLOPS) and MegaFLOPS (MFLOPS), model size is expressed in Megabytes (MB), the number of parameters is represented in Millions (M), and inference time is measured in milliseconds (ms).

TABLE IV: Comparison of proposed 3D CNN model complexity and computational resource for various configurations.

# of Proposed 3D CNN Blocks	Metrics	Features		
		RE	RA	RE+RA
1	**#Parameter (M)**	83.8	83.8	83.8
	Inference Time (ms)	7.82	7.78	10.36
	#Flops (MFLOPS)	312	311	453.5
	Model Size (MB)	640	640	640
	Memory Usage (MB)	424.11	425.92	561.78
2	**#Parameter (M)**	16.8	16.8	16.8
	Inference Time (ms)	9.84	8.04	9.50
	#Flops (GFLOPS)	1.3	1.3	1.4
	Model Size (MB)	128	128	128
	Memory Usage (MB)	432.77	436.41	573.14
3	**#Parameter (M)**	4.4	4.4	4.4
	Inference Time (ms)	10.09	9.17	9.28
	#Flops (GFLOPS)	1.7	1.7	1.8
	Model Size (MB)	34.2	34.2	34.2
	Memory Usage (MB)	433.25	433.98	570.39

Our experimental results lead to several key findings:

- The integration of elevation and azimuth data is crucial for achieving robust fall detection performance. While increasing the number of 3D CNN blocks does not substantially enhance accuracy, it improves training convergence and reduces the total parameter count.
- System designers must carefully balance the trade-offs between model complexity and computational efficiency, considering specific deployment constraints and accuracy requirements.

These insights provide valuable guidance for optimizing fall detection systems across various operational scenarios and resource constraints.

IV. Conclusion and Future Work

This study introduces a system optimized for AAL environments, combining FMCW radar technology with deep learning for effective, reliable, and cost-effective fall detection. By

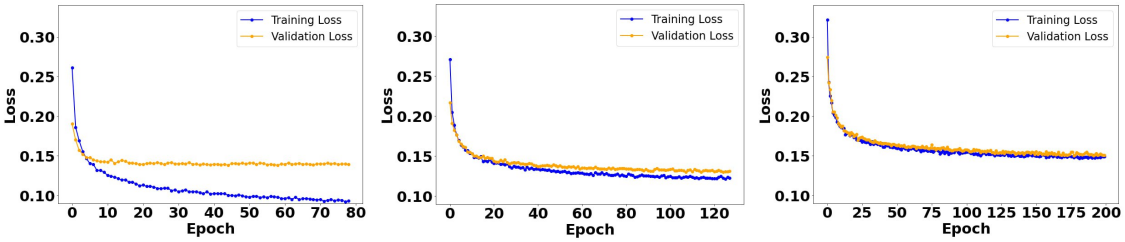

(a) One 3D CNN block. (b) Two 3D CNN blocks. (c) Three 3D CNN blocks.

Fig. 5: Training loss for different proposed model configurations and RE+RA feature input.

utilizing two wall-mounted mmWave radars, the system captures human motion data across various positions in the room, transforming it into RA and RE maps, which serve as feature vectors for a 3D CNN model. The proposed model achieved high accuracy, with a rate of 94.33% and a macro F1-score of 93.5%, thereby balancing reliability and generalizability. Our findings underscore the advantages of integrating range, azimuth, and elevation data, demonstrating the effectiveness of 3D CNN architecture in capturing both temporal and spatial features for an enhanced fall detection system.

Future research could build upon this work by exploring additional environmental configurations and optimizing real-time processing capabilities for deployment in varied AAL contexts. With robust detection performance under diverse lighting conditions and a strong commitment to user privacy, this system offers a scalable solution for elderly care, with significant potential to enhance safety and quality of life.

REFERENCES

[1] N. T. Newaz and E. Hanada, "The methods of fall detection: A literature review," *Sensors*, vol. 23, no. 11, 2023. [Online]. Available: https://www.mdpi.com/1424-8220/23/11/5212

[2] N. Pannurat, S. Thiemjarus, and E. Nantajeewarawat, "Automatic fall monitoring: A review," *Sensors*, vol. 14, no. 7, pp. 12 900–12 936, 2014.

[3] M. Li, P. Li, S. Tian, K. Tang, and X. Chen, "Estimation of temporal gait parameters using a human body electrostatic sensing-based method," *Sensors (Switzerland)*, vol. 18, 6 2018.

[4] I. Ullmann, R. G. Guendel, N. C. Kruse, F. Fioranelli, and A. Yarovoy, "A survey on radar-based continuous human activity recognition," *IEEE Journal of Microwaves*, vol. 3, pp. 938–950, 7 2023.

[5] J. Hasch, E. Topak, R. Schnabel, T. Zwick, R. Weigel, and C. Waldschmidt, "Millimeter-wave technology for automotive radar sensors in the 77 ghz frequency band," *IEEE Transactions on Microwave Theory and Techniques*, vol. 60, no. 3, pp. 845–860, 2012.

[6] H. Abedi, A. Ansariyan, C. Lehman, P. P. Morita, J. Boger, and A. Wong, "Non-visual and contactless wellness monitoring for long term care facilities using mm-wave radar sensors," in *2022 IEEE Sensors Conference*, Dallas, TX, USA, Oct 2022.

[7] H. Abedi, A. Ansariyan, P. P. Morita, J. Boger, A. Wong, and G. Shaker, "Sequential deep learning for in-home activity monitoring using mm-wave fmcw radar," in *2021 IEEE International Symposium on Antennas and Propagation and USNC-URSI Radio Science Meeting (APS/URSI)*, Singapore, Singapore, Dec 2021.

[8] H. Abedi, J. Boger, P. P. Morita, A. Wong, and G. Shaker, "Hallway gait monitoring using novel radar signal processing and unsupervised learning," *IEEE Sensors Journal*, vol. 22, pp. 15 133–15 145, 8 2022.

[9] H. Abedi, J. Boger, P. Morita, A. Wong, and G. Shaker, "Hallway gait monitoring system using an in-package integrated dielectric lens paired with a mm-wave radar," *Sensors*, vol. 23, no. 1, p. 71, Jan 2023.

[10] Y. Yao, C. Liu, H. Zhang, B. Yan, P. Jian, P. Wang, L. Du, X. Chen, B. Han, and Z. Fang, "Fall detection system using millimeter-wave radar based on neural network and information fusion," *IEEE Internet of Things Journal*, vol. 9, no. 21, pp. 21 038–21 050, 2022.

[11] M. Alizadeh, G. Shaker, J. C. M. D. Almeida, P. P. Morita, and S. Safavi-Naeini, "Remote monitoring of human vital signs using mm-wave fmcw radar," *IEEE Access*, vol. 7, pp. 54 958–54 968, 2019.

[12] "Bgt60tr13c - xensiv™ 60ghz radar sensor for advanced sensing," https://www.infineon.com/cms/en/product/sensor/radar-sensors/radar-sensors-for-iot/60ghz-radar/bgt60tr13c/, 2023.

[13] B. Erol, M. Amin, Z. Zhou, and J. Zhang, "Range information for reducing fall false alarms in assisted living," in *2016 IEEE Radar Conference (RadarConf)*, 2016, pp. 1–6.

[14] M. Shen, K.-L. Tsui, M. A. Nussbaum, S. Kim, and F. Lure, "An indoor fall monitoring system: Robust, multistatic radar sensing and explainable, feature-resonated deep neural network," *IEEE Journal of Biomedical and Health Informatics*, vol. 27, no. 4, pp. 1891–1902, 2023.

[15] S. S. Khan and J. Hoey, "Review of fall detection techniques: A data availability perspective," *Medical Engineering & Physics*, vol. 39, pp. 12–22, 2017. [Online]. Available: https://www.sciencedirect.com/science/article/pii/S1350453316302600

[16] S.-G. Miaou, P.-H. Sung, and C.-Y. Huang, "A customized human fall detection system using omni-camera images and personal information," in *1st Transdisciplinary Conference on Distributed Diagnosis and Home Healthcare, 2006. D2H2.*, 2006, pp. 39–42.

[17] J. Fleming and C. Brayne, "Inability to get up after falling, subsequent time on floor, and summoning help: prospective cohort study in people over 90," *Bmj*, vol. 337, 2008.

[18] S. Jardak, T. Kiuru, M. Metso, P. Pursula, J. Häkli, M. Hirvonen, S. Ahmed, and M.-S. Alouini, "Detection and localization of multiple short range targets using fmcw radar signal," in *2016 Global Symposium on Millimeter Waves (GSMM) & ESA Workshop on Millimetre-Wave Technology and Applications*, 2016, pp. 1–4.

[19] C. Lovescu and S. Rao, "The fundamentals of millimeter wave radar sensors," *Texas Instruments, Julio*, 2020.

[20] X. Zeng, H. S. L. Báruson, and A. Sundvall, "Walking step monitoring with a millimeter-wave radar in real-life environment for disease and fall prevention for the elderly," *Sensors*, vol. 22, no. 24, p. 9901, 2022.

[21] H. Abedi, C. Magnier, V. Mazumdar, and G. Shaker, "Improving passenger safety in cars using novel radar signal processing," *Engineering Reports*, vol. 3, 12 2021.

[22] C. Will, P. Vaishnav, A. Chakraborty, and A. Santra, "Human target detection, tracking, and classification using 24-ghz fmcw radar," *IEEE Sensors Journal*, vol. 19, no. 17, pp. 7283–7299, 2019.

[23] H. Abedi, A. Ansariyan, P. P. Morita, A. Wong, J. Boger, and G. Shaker, "Ai-powered noncontact in-home gait monitoring and activity recognition system based on mm-wave fmcw radar and cloud computing," *IEEE Internet of Things Journal*, vol. 10, pp. 9465–9481, 6 2023.

[24] Z. Zhang, Z. Tian, and M. Zhou, "Latern: Dynamic continuous hand gesture recognition using fmcw radar sensor," *IEEE Sensors Journal*, vol. 18, no. 8, pp. 3278–3289, 2018.

[25] W. Li, D. Zhang, Y. Li, Z. Wu, J. Chen, D. Zhang, Y. Hu, Q. Sun, and Y. Chen, "Real-time fall detection using mmwave radar," in *ICASSP 2022 - 2022 IEEE International Conference on Acoustics, Speech and Signal Processing (ICASSP)*, 2022, pp. 16–20.

[26] W. Li, W. Wang, D. Zhang, and Gegentuya, "Human motion recognition method using millimeter-wave radar based on 3dtsnet," in *2023 5th International Conference on Electronics and Communication, Network and Computer Technology (ECNCT)*, 2023, pp. 18–22.